

THERMAL AND FLUID DYNAMIC ANALYSIS OF SOLAR CHIMNEY BUILDING SYSTEMS

Bernardo Buonomo, Oronzio Manca, Sergio Nardini, Paolo Romano

Dipartimento di Ingegneria Industriale e dell'Informazione, Seconda Università degli Studi di Napoli,
Via Roma 29, 81031 Aversa (CE), Italy

ABSTRACT

In this paper a numerical investigation on a prototypal solar chimney system integrated in a south facade of a building is presented. The analysis is carried out on a three-dimensional model in air flow and the governing equations are given in terms of k - ϵ turbulence model. Two geometrical configurations are investigated: 1) a channel with principal walls one vertical and the other inclined and 2) a channel with vertical parallel walls. The chimney is 4.0 m high, 1.5 m wide whereas the thickness is 0.20 m for the vertical parallel walls configuration and at the inlet 0.34 m and at the outlet 0.20 m for the inclined ones. The problem is solved by means of the commercial code Ansys-Fluent and the results are performed for an uniform wall heat flux on the vertical wall equal to 300 and 600 W/m². Results are given in terms of wall temperature distributions, air velocity and temperature fields and transversal profiles in order to evaluate the differences between the two base configurations and thermal and fluid dynamic behaviors. Further, the ground effect on thermal performances is examined and discussed.

1. INTRODUCTION

The increase in world population and the improvement of living standards have led to a growing demand for electricity. The limited availability of fossil fuels and environmental pollution caused by them, push the development of new technologies for the production of electricity from renewable energy sources. With a view to sustainable development, therefore, the energy future must have as protagonists renewable sources (solar, geothermal, wind, etc.), which are not exhausted and have no environmental impact because they do not produce greenhouse gases.

Buildings as big energy-consuming systems require large amount of energy to operate. Globally, buildings are responsible for approximately 40% of total world annual energy consumption. Sustainable design and construction are gaining significant momentum in the construction industry. Designers and owners are learning that with smart design, buildings can save energy and have a decreased impact on the environment. Sustainable buildings with renewable energy systems are trying to operate independently without consumption of conventional resources. This reduces impact on the environment throughout buildings' lifecycle. Renewable energy is a significant approach to reduce resource consumption in sustainable building [1] and integrated solar chimney systems could represent a possible solution [2].

A solar chimney is essentially divided into two parts, one – the solar air heater (collector) and second – the chimney. Two configurations of solar chimney are usually used: vertical solar chimney with vertical absorber geometry, and roof solar chimney [3]. For vertical solar chimney, vertical glass is used to gain solar heat. Temperature difference between vertical glass duct and interior room produces a pressure difference. An interior air will go out through inlet because of this pressure difference. The temperature difference is a

determining factor of performance of solar chimney [4].

Designing a solar chimney includes height, width and depth of cavity, type of glazing, type of absorber, and inclusion of insulation or thermal mass. Besides these system parameters, other factors such as the location, climate, and orientation can also affect its performance [5-7].

The solar chimney power plant uses solar radiation to raise the temperature of the air and the buoyancy of warm air to accelerate the air stream flowing through the system. This is an energy conversion system from solar to mechanical. A component, such as a turbine, set in the path of the air current, converts the kinetic energy of the flowing air into electricity.

Schlaich [8] in the late 1970s was the first to propose the solar chimney concept. Less than 4 years after he presented his ideas at a conference, construction on a pilot plant began in Manzanares, Spain, as a result of a joint venture between the German government and a Spanish utility. A 36 kW pilot plant was built, which produced electricity for 7 years, thus proving the efficiency and reliability of this novel technology. The chimney tower was 194.6 m high, and the collector had a radius of 122 m. Haaf [9] reported fundamental investigations, design criteria, and cost analysis for the Spanish system. Bernardes [10] presented a theoretical analysis of a solar chimney, operating on natural laminar convection in steady state. Von Backström and Fluri [11] investigated analytically the validity and applicability of the assumption that, for maximum fluid power. Von Backström and Gannon [12] were interested mainly in a one-dimensional compressible flow for the thermodynamic variable as dependence on chimney height, wall friction, additional losses, internal drag and area exchange. Pretorius and Kröger [13] evaluated the influence of a developed convective heat transfer equation, more accurate turbine inlet loss coefficient, quality collector roof glass and various types of soil on the performance of a large scale solar chimney power plant. Ming et al. [14] presented a

mathematical model to evaluate the relative static pressure and driving force of the solar chimney power plant system and verified the model with numerical simulations. Maia et al. [15] presented a theoretical analysis of a turbulent flow inside a solar chimney. They showed that the most important physical elements in a solar chimney system are the tower dimensions as they cause the most significant variation in the flow behavior. Tahar and Mahfoud [16] presented a numerical simulation of natural convection in a solar chimney. They examined the effect of the system geometry on the natural convection phenomenon in the solar chimney.

In this paper a numerical investigation on a prototypal solar chimney system integrated in a south facade of a building is presented. The analysis is carried out on a three-dimensional model in air flow and the governing equations are given in terms of k-ε turbulence model. The problem is solved by means of the commercial code Ansys-Fluent and the results are performed for a uniform wall heat flux on the vertical wall is equal to 300 and 600 W/m². Results are given in terms of wall temperature distributions, air velocity and temperature fields and transversal profiles in order to evaluate the differences between the two base configurations and thermal and fluid dynamic behaviors. Further, the ground effect on thermal performances is also examined.

NOMENCLATURE

L	channel high, m
H	ground distance, m
W	channel width, m
b _{min}	thickness outlet, m
b _{max}	thickness inlet, m
C _p	Specific heat at constant pressure, J/Kg·K
C _{1ε} , C _{2ε} , C _μ	Empirical constants in the k - ε turbulence model
D	Extra term in Eq. 7
E	Roughness parameter
f ₁ , f ₂ , f _μ	Wall damping function
g	Gravitational constant, m/s ²
G _b	Production of turbulent kinetic energy due to buoyancy
G _k	Production of turbulent kinetic energy due to mean velocity gradient
Gr	Grashof number
h	Average heat transfer co-efficient, W/m ² ·K
h _y	Local heat transfer coefficient, W/m ² ·K
k	Kinetic energy of turbulence
Nu _y	Local Nusselt number
Nu	Average Nusselt number
p	Pressure, Pa
q	Heat flux, W/m ²
Pr	Prandtl number
Pr _t	Turbulent Prandtl number
Ra	Rayleigh number = (GrPr)
T	Temperature, K
T _o	Ambient temperature, K
T _s	Channel wall (surface) temperature, K
u, v, w	x-, y- and z-components of velocities, respectively, m/s
$\bar{u}, \bar{v}, \bar{w}$	Time-averaged x, y and z components of velocities, respectively
X, Y, Z	Cartesian coordinates

Greek symbols

α	Thermal diffusivity, m ² /s
β	Co-efficient of thermal expansion, K ⁻¹
κ	Thermal conductivity, W/m·K
ε	Rate of dissipation of the kinetic energy
μ	Laminar viscosity, Pa·s
μ _t	Turbulent viscosity, Pa·s
ν	Molecular kinematic viscosity, m ² /s ⁻¹
ρ	Density, Kg/m ³
σ _k	Prandtl number for k
σ _ε	Prandtl number for ε

2. MATHEMATICAL MODEL

The present study considers steady, turbulent, three-dimensional natural convection flow in a solar chimney as shown in Fig. 1.

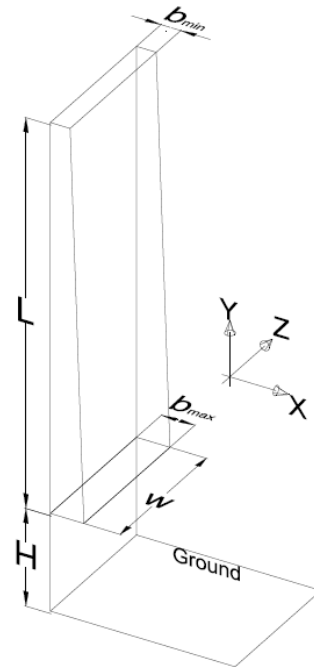


Figure 1. Geometry configuration.

All the thermophysical fluid properties are assumed to be invariant except for the density in the buoyancy force term which can be adequately modeled by the Boussinesq approximation. The compression work, viscous dissipation and radiative transport are assumed to be negligibly small. Thus, the governing equations can be written as:

Conservation of mass

$$\frac{\partial \rho}{\partial t} + \rho \cdot \nabla \cdot \vec{V} = 0 \quad (1)$$

Conservation of x-momentum

$$\rho \frac{Du}{Dt} = \rho f_x - \frac{\partial p}{\partial x} + \frac{\partial \tau_{xx}}{\partial x} + \frac{\partial \tau_{yx}}{\partial y} + \frac{\partial \tau_{zx}}{\partial z} \quad (2)$$

Conservation of y-momentum

$$\rho \frac{Dv}{Dt} = \rho f_y - \frac{\partial p}{\partial y} + \frac{\partial \tau_{xy}}{\partial x} + \frac{\partial \tau_{yy}}{\partial y} + \frac{\partial \tau_{zy}}{\partial z} \quad (3)$$

Conservation of z-momentum

$$\rho \frac{Dw}{Dt} = \rho f_z - \frac{\partial p}{\partial z} + \frac{\partial \tau_{xz}}{\partial x} + \frac{\partial \tau_{yz}}{\partial y} + \frac{\partial \tau_{zz}}{\partial z} \quad (4)$$

Conservation of Energy

$$\rho \cdot_p \frac{DT}{Dt} = k \nabla^2 T + \mu_t \Phi + u''' \quad (5)$$

Where μ is the turbulent dynamic viscosity which is calculated from the knowledge of the kinetic energy of turbulence, k , and turbulent kinetic energy dissipation rate, ε , as follows

$$\mu_t = \rho C_{\mu} f_{\mu} \left(\frac{k^2}{\varepsilon} \right) \quad (6)$$

Turbulence kinetic energy (k -equation)

$$\begin{aligned} \frac{\partial}{\partial x} (\rho \bar{u} k) + \frac{\partial}{\partial y} (\rho \bar{v} k) + \frac{\partial}{\partial z} (\rho \bar{w} k) &= \frac{\partial}{\partial x} \left[\left(\mu + \frac{\mu_t}{\sigma_k} \right) \frac{\partial k}{\partial x} \right] \\ + \frac{\partial}{\partial y} \left[\left(\mu + \frac{\mu_t}{\sigma_k} \right) \frac{\partial k}{\partial y} \right] + \frac{\partial}{\partial z} \left[\left(\mu + \frac{\mu_t}{\sigma_k} \right) \frac{\partial k}{\partial z} \right] & \quad (7) \\ + G_k + G_b - \rho \varepsilon - D \end{aligned}$$

Turbulence dissipation (ε -equation)

$$\begin{aligned} \frac{\partial}{\partial x} (\rho \bar{u} \varepsilon) + \frac{\partial}{\partial y} (\rho \bar{v} \varepsilon) + \frac{\partial}{\partial z} (\rho \bar{w} \varepsilon) &= \frac{\partial}{\partial x} \left[\left(\mu + \frac{\mu_t}{\sigma_{\varepsilon}} \right) \frac{\partial \varepsilon}{\partial x} \right] \\ + \frac{\partial}{\partial y} \left[\left(\mu + \frac{\mu_t}{\sigma_{\varepsilon}} \right) \frac{\partial \varepsilon}{\partial y} \right] + \frac{\partial}{\partial z} \left[\left(\mu + \frac{\mu_t}{\sigma_{\varepsilon}} \right) \frac{\partial \varepsilon}{\partial z} \right] & \quad (8) \\ + C_{\varepsilon 1} f_1 \frac{\varepsilon}{k} (G_k + G_{\varepsilon 3} G_b) - C_{\varepsilon 2} f_2 \frac{\varepsilon^2}{k} + E \end{aligned}$$

In the k and ε Eqs.(7) and (8), the first two terms represent transport of kinetic energy of turbulence or dissipation rate of kinetic energy by convection. Third and fourth terms represent transport of these quantities by diffusion. G_k represents the rate of generation of turbulent kinetic energy due to mean velocity gradients, $\rho \varepsilon$, is the destruction rate of the turbulent kinetic energy and G_b is the rate of generation of turbulent kinetic due to buoyancy. In addition, there are some extra terms denoted by D in k -equation and E in ε -equation to account for near wall behavior. f_1 and f_2 are the wall damping functions in ε -equation [17].

The geometry under consideration in this analysis is constituted by a convergent vertical channel. The channel is formed by a vertical surface of height L , on which is imposed an uniform heat flux, and by an inclined surface of 2° from the

vertical. The inlet and the outlet section of the channel are b_{\max} and b_{\min} respectively, while the depth is equal to w . H is the distance from the ground of the input section.

The CAD model and the step of preprocessing were realized with software Gambit.

The boundary conditions imposed at the solid walls are mainly the no-slip and impermeability boundary conditions in addition to the specified wall heat flux. The conditions assumed at the inlet and outlet sections are those of ambient conditions (ambient pressure and temperature)

Table 1. Geometric parameters.

L	4.00 m
H	1.00 m
b_{\max}	0.34 m
b_{\min}	0.20 m
w	1.50 m

3. THE NUMERICAL SOLUTION

The governing equations given represent a set of coupled, non-linear, elliptic partial differential equations. In the present study, the numerical solutions of these were carried out using the commercial code FLUENT 6.3[18]. The operating temperature was set equal to 300 K; the acceleration of gravity was considered, and its value was set equal to 9.81 m/s^2 . All the non-heated surfaces were considered adiabatic whereas in the first analysis an uniform heat flux of 300 W/m^2 and 600 W/m^2 on the heated surface was considered. The first simulations have the purpose to analyze the sensitivity of the grid on the numerical solution. In this paper a study on a different grid models has been carried out. Table 2 shows the grids analyzed. Richardson's equation, Eq. (9), allows us to estimate the exact value of a generic quantity comparing two configurations at a time.

$$f_{\text{exact}} = \frac{4}{3} f_{i+1} - \frac{1}{3} f_i \quad (9)$$

After which it is possible to estimate the percentage error with the Eq. (10).

$$e\% = \frac{f_i - f_{i+1}}{f_{i+1}} \quad (10)$$

For each grid was evaluated the value of the average Nusselt number of vertical surface. The Fig. 2 shows the percentage error of Nusselt number. Therefore the grid 3 was used in this study, because it presented a percentage error of Nusselt number equal to 1.13% with computational saving compared to grid 4 and 5.

Table 2. Analyzed grids.

GRID	ELEMENTS
1	54157
2	334552
3	433256
4	860064
5	3433932

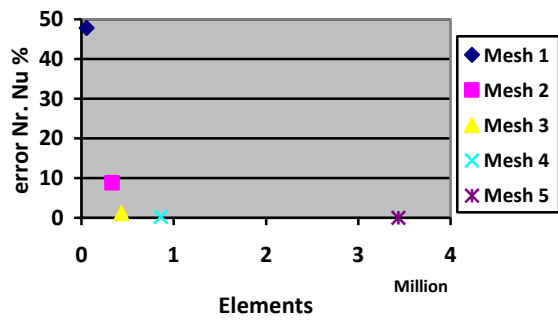


Figure 2. Percentage error Nusselt number.

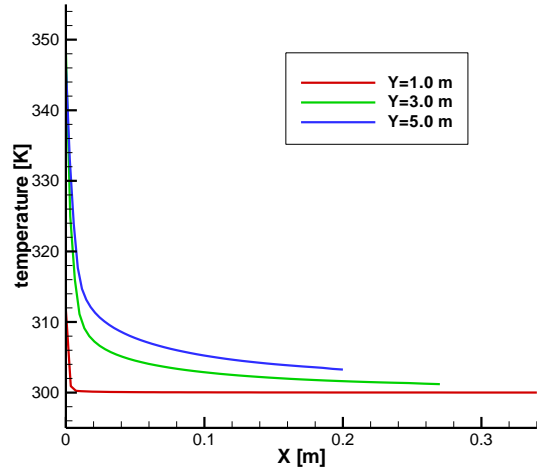


Figure 4. Air Temperature profile in the channel spacing, at the mid-channel section ($Z=0.75$ m) and several heights for $q=300$ W/m^2 .

4. RESULTS AND DISCUSSION

4.1 Heat flux effect

The main aim is to analyze the heat flux effect on heat transfer and air flow into the chimney. For this reason, the fields and the profiles of air temperature and velocity are presented.

Figure 3 shows temperature distribution on the heated vertical surface for a heat flux equal to 300 W/m^2 .

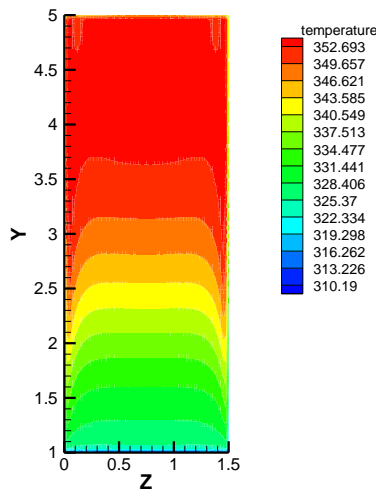


Figure 3. Temperature field of the vertical surface for $q=300$ W/m^2 .

Wall temperature increases from the bottom upwards due to the progressive heating of the air in the channel. Furthermore, it can be seen also that the temperature assumes a uniform value, about 350 K downstream the middle of channel height. Air temperature in the channel grows from bottom to up, by presenting the highest values near the heated wall, as shown in Fig.4, where the temperature profiles along the transversal sections at $Z=0.75$ m and $Y=1.0, 3.0$ and 5.0 m.

Figure 5 shows the distribution of the Nusselt number on the vertical heated wall. It decreases from bottom to up due to convective heat transfer reduction. Figure 6 reports the profile of local Nusselt number on the centerline of the heated wall, and its value varies from 98 to 38 . Average Nusselt number is equal to 53.8 . The air velocity, in Fig. 7, increases from bottom to up due to the convergence of principal walls in the solar chimney. Velocity profiles at three different heights, $Y=1.0, 3.0, 5.0$ m, are reported in Fig. 8, for $Z = 0.75$ m. It is noted that the maximum is reached in the outlet section in

proximity of the vertical wall and its value is equal to 0.92 m/s. Another important parameter evaluated in this study is the air mass flow rate and, in these conditions, it is equal to 227 g/s. In Tab. 3, the main parameter values are summarized.

Increasing the heat flux from 300 W/m^2 to 600 W/m^2 temperature and velocity fields are very similar, but in this last case their values are higher than the previous one, Figs 9-13. Local Nusselt number on the centerline of the heated wall decreases from 103 to 50 . Average Nusselt number is equal to 60.9 and mass flow rate is equal to 289 g/s. Table 4 summarizes the main parameter values.

Table 3. Values of the significant parameters for $q=300$ W/m^2 .

	H= 1.0 m
Heat flux [W/m^2]	300
Average Nusselt number	53.8
Mass flow rate [g/s]	227
V_{max} [m/s]	0.92
T_{max} [K]	357

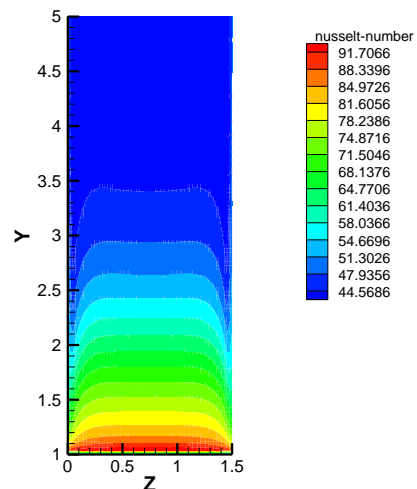


Figure 5. Nusselt number distribution on the vertical heated wall for $q=300$ W/m^2 .

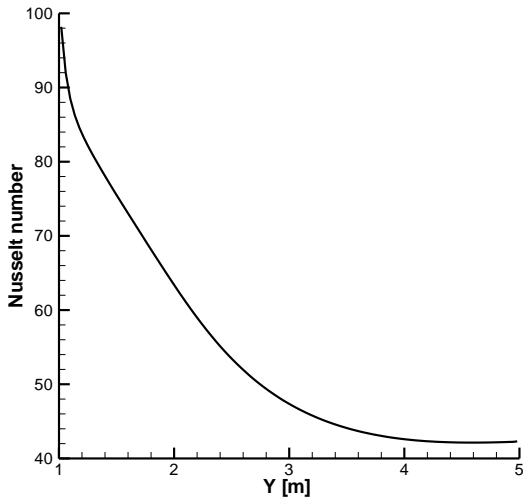


Figure 6. Local Nusselt number on the heated wall, at the mid-channel section ($Z=0.75$ m) for $q=300$ W/m^2 .

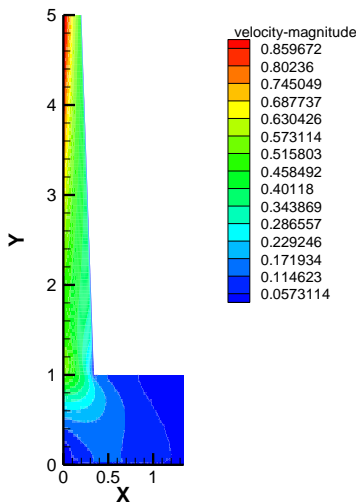


Figure 7. Velocity magnitude field, at the mid-channel section ($Z=0.75$ m) for $q=300$ W/m^2 .

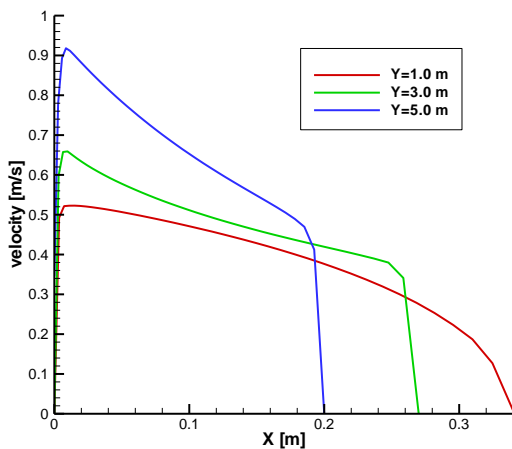


Figure 8. Velocity magnitude profiles in the channel spacing, at the mid-channel section ($Z=0.75$ m) and several heights for $q=300$ W/m^2 .

Table 4. Values of the significant quantities for $q=600$ W/m^2 .

	H= 1.0 m
Heat flux [W/m^2]	600
Average Nusselt number	60.9
Mass flow rate [g/s]	289
V_{max} [m/s]	1.18
T_{max} [K]	395

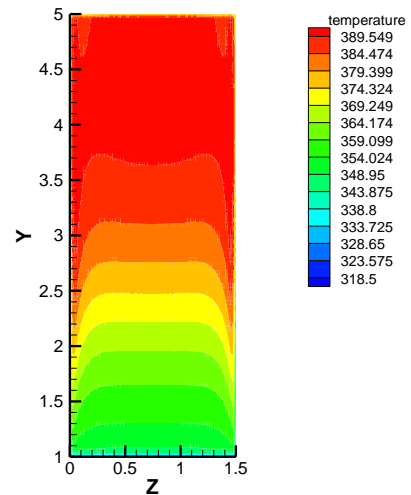


Figure 9. Temperature field vertical surface for $q=600$ W/m^2 .

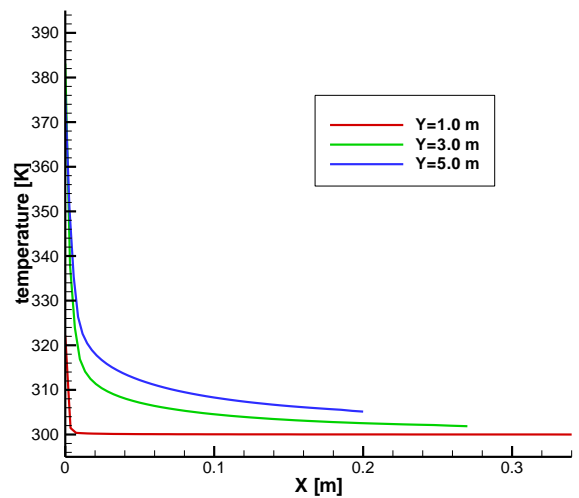


Figure 104. Air Temperature profile in the channel spacing, at the mid-channel section ($Z=0.75$ m) and several heights for $q=600$ W/m^2 .

In Figs. 14-15, a comparison between the two cases is reported in terms of heated wall temperature along the heated wall centerline and velocity at the outlet section along the X coordinate for $Y=5.0$ m and $Z=0.75$ m. It is noticed that doubling the wall heat flux there is an increase of almost 30% of the mass flow rate, of almost 30% of the maximum air velocity and about 10% of the maximum heated wall temperature. In Table 5, the main parameter values are shown for the two heat flux.

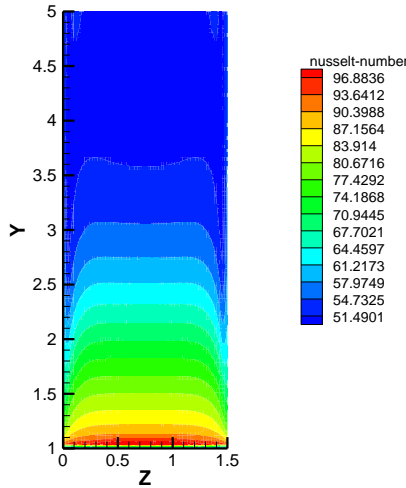


Figure 11. Nusselt number distribution on the vertical heated wall for $q=600 \text{ W/m}^2$.

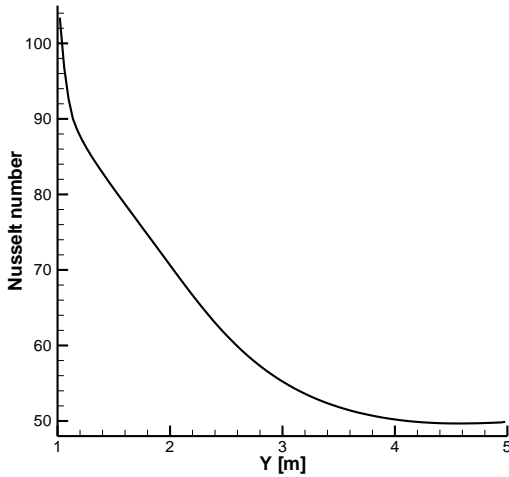


Figure 12. Local Nusselt number on the heated wall, at the mid-channel section ($Z=0.75 \text{ m}$) for $q=600 \text{ W/m}^2$.

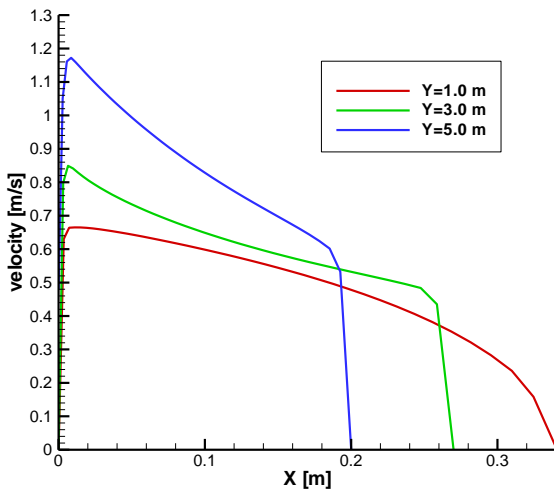


Figure 13. Velocity magnitude profile in the channel spacing, at the mid-channel section ($Z=0.75 \text{ m}$) and several heights for $q=600 \text{ W/m}^2$.

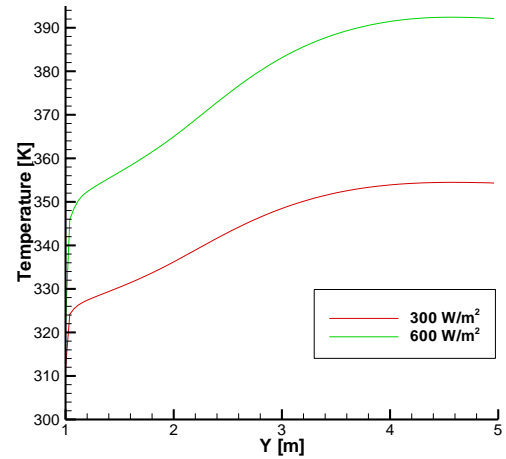


Figure 14. Comparison of centerline heated wall temperature.

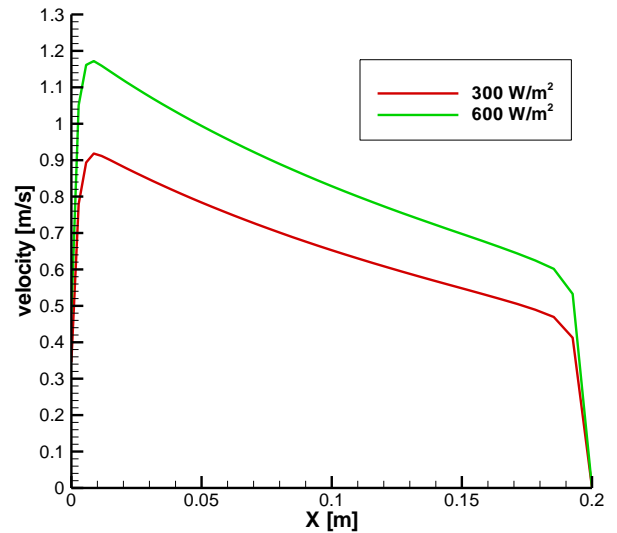


Figure 15. Comparison of outlet magnitude velocity.

Table 5. Comparison between the significant quantities for $q=300$ and 600 W/m^2 .

	H= 1.0 m	H= 1.0 m
Heat flux [W/m^2]	300	600
Average Nusselt number	53.8	60.9
Mass flow rate [g/s]	227	289
V_{max} [m/s]	0.92	1.18
T_{max} [K]	357	395

4.2 Geometry parameters effect

In this paragraph, the geometry effect on solar chimney is evaluated considering a channel with vertical parallel walls. The thickness is equal to 0.20 m while all other parameters are equal to the previous case.

Figures 16 shows the field of temperature of vertical surface in case of heat flux equal to 300 W/m^2 . Also in this case it is noted that the temperature increases from bottom to top for the progressive heating of the air, assuming a uniform value, about 350 K, at mid-wall. The air temperature, in the channel, grows from bottom to up, presenting the highest values near the heated wall, Fig. 17.

The distribution of the Nusselt number on the vertical surface is reported in Fig. 18, it is noted that it decreases from the bottom upwards due to the reduction of the convective heat transfer. Fig. 19 reports the local Nusselt number profile along the heated wall centerline and its value varies from 117 to 42. Average Nusselt number is equal to 52.9. The maximum air velocity increases from bottom to up, in the solar chimney, due to air heating close to the heated wall, as reported in Fig. 19. In figure velocity profiles, for three different values of Y , are given. The maximum air velocity is equal to 0.88 m/s and the mass flow rate of air is equal to 185 g/s. Table 6 summarizes the main parameter values.

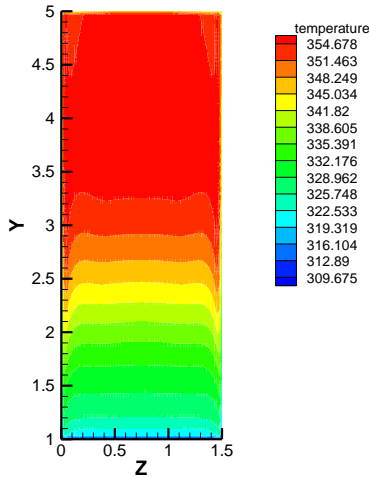


Figure 16. Temperature field vertical surface for parallel walls and $q=300 \text{ W/m}^2$.

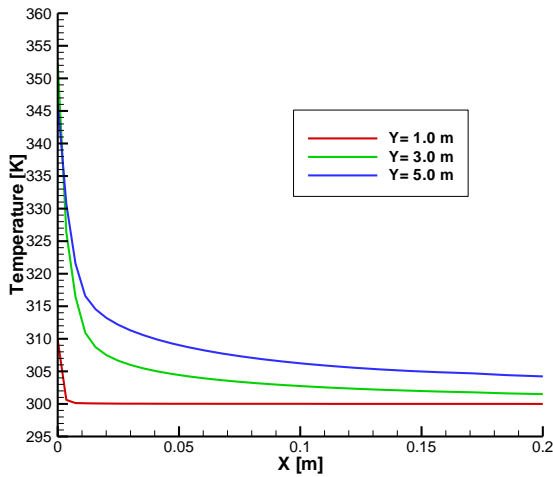


Figure 5. Air Temperature profile in the channel spacing, at the mid-channel section ($Z=0.75 \text{ m}$) and several heights for parallel walls and $q=300 \text{ W/m}^2$.

Table 6. Values of the significant quantities for parallel walls and $q=300 \text{ W/m}^2$.

	H= 1.0 m
Heat flux [W/m^2]	300
Average Nusselt number	52.89
Mass flow rate [g/s]	185
V_{\max} [m/s]	0.82
T_{\max} [K]	358

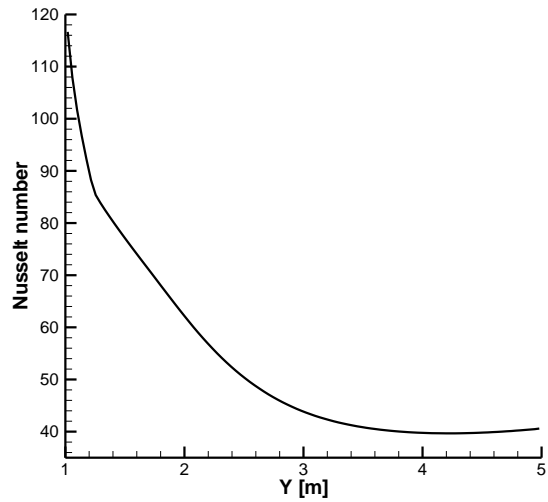


Figure 186. Local Nusselt number on the heated wall, at the mid-channel section ($Z=0.75 \text{ m}$) for parallel walls $q=300 \text{ W/m}^2$.

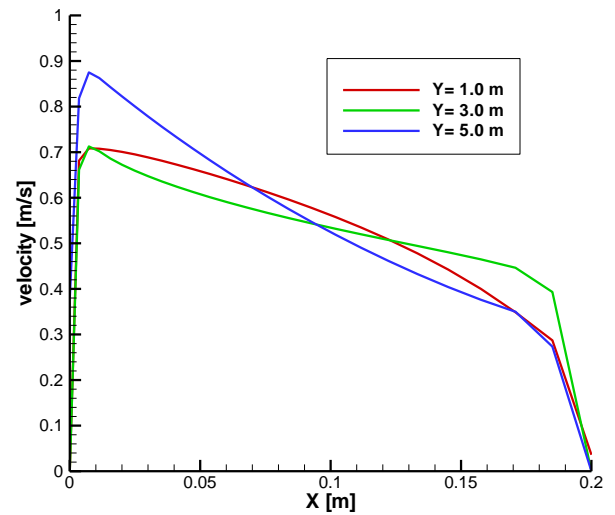


Figure 19. Velocity magnitude profile in the channel spacing, at the mid-channel section ($Z=0.75 \text{ m}$) and several heights for parallel walls and $q=300 \text{ W/m}^2$.

Comparing the two different geometrical configurations from a thermal point of view, the behavior is similar whereas some changes are related to the fluid dynamic behaviors. In Fig. 20, it is possible to observe that wall temperatures profiles are very similar. While, in Fig. 21, air velocity in the outlet section of converging channel is higher than the one in straight duct.

5. CONCLUSIONS

At an assigned distance from the ground and analyzing the phenomenon for different heat fluxes, is observed an increase of the values of temperature, velocity and mass flow rate with increasing heat flux of wall. Especially doubling the thermal flux, from 300 W/m^2 to 600 W/m^2 there is an increase of almost 30% of the mass flow in the outlet section of the duct; an increase of almost 30% of the maximum velocity of the fluid, and approximately 10% of the maximum temperature of the heated wall.

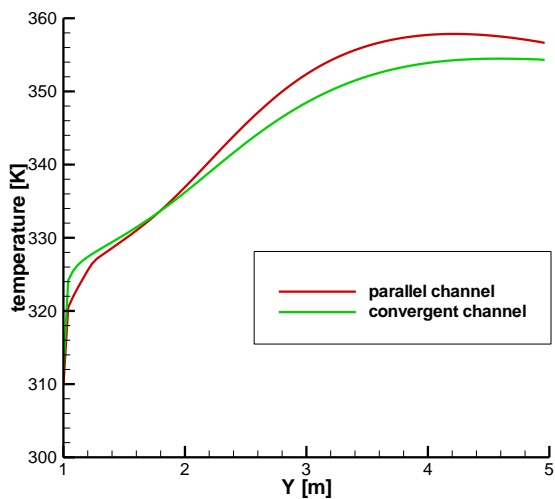


Figure 20. Comparison of centerline heated wall temperature.

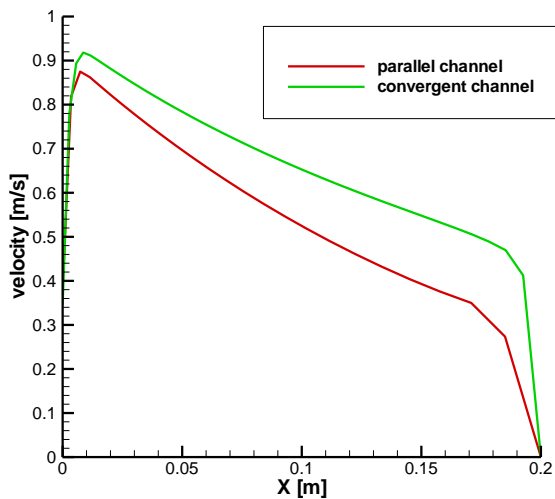


Figure 21. Comparison of outlet magnitude velocity.

The numerical investigation carried out with the purpose of verifying the effect of the geometry of the chimney on the investigated parameters, showed as a straight chimney in place of a convergent does not lead to substantial differences from the thermal point of view and from the investigated fluid. In particular it passes from a maximum speed of 0.92 m/s for the converging channel to 0.88 m/s for the straight duct, therefore a reduction of approximately 5%, while the mass flow is reduced by about 20%, from 227 g/s to 185 g/s.

REFERENCES

1. J. Arce, J.P. Xamán, G. Álvarez, M.J. Jiménez, R. Enríquez and M.R. Heras, A Simulation of the Thermal

- Performance of a Small Solar Chimney Already Installed in a Building, ASME 2010 4th International Conference on Energy Sustainability, ES 2010 2 , pp. 337-347, 2010.
2. M. Najmi, A. Nazari, H. Mansouri, G. Zahedi, Feasibility study on optimization of a typical solar chimney power plant, Heat and Mass Transfer 48 (3) , pp. 475-485, 2011.
3. A. Asnaghi, S.M. Ladjevardi, Solar chimney power plant performance in Iran, Renewable and Sustainable Energy Reviews 16 (5), pp. 3383-3390, 2012.
4. E. Gholamalizadeh and S. H. Mansouri, A comprehensive approach to design and improve a solar chimney power plant: A special case - Kerman project, Applied Energy 102 , pp. 975-982, 2013.
5. J. Li, P. Guo, Y. Wang, Effects of collector radius and chimney height on power output of a solar chimney power plant with turbines, Renewable Energy 47 , pp. 21-28, 2012.
6. A.Y.K. Tan and N.H. Wong, Parameterization Studies of Solar Chimneys in the Tropics, Energies 6 (1), pp. 145-163 2013.
7. A. Koonsrisuk, T. Chitsomboon, Effects of flow area changes on the potential of solar chimney power plants, Energy 51 , pp. 400-406, 2013.4
8. J. Schlaich, The Solar Chimney: Electricity from the Sun, Edition Axel Menges, Stuttgart, Germany, 1995.
9. W. Haaf, K. Friedrich, G. Mayer, J. Schlaich, Solar chimneys, Part I: principle and construction of the pilot plant in Manzanares, International Journal of Solar Energy 2, pp. 3-20, 1983.
10. M.A. Bernardes, S. Dos, R.M. Valle, M.F.B. Cortez, Numerical analysis of natural laminar convection in a radial solar heater, International Journal of Thermal Science 38, pp. 42-50, 1999.
11. T.W. Von Backström, TP. Fluri, Maximum fluid power condition in solar chimney power plants-an analytical approach, Solar Energy 80, pp. 1417-1423, 2006.
12. T.W. Von Backstrom, A.J. Cannon, Compressible flow through solar power plant chimneys, Journal of Solar Energy Engineering 122, pp. 138-145, 2000.
13. J.P. Pretorius, D.G. Kröger, Critical evaluation of solar chimney power plant performance, Solar Energy 80, pp. 535-544, 2006.
14. T.Z. Ming, W. Liu, G.L. Xu, A.W. Fan, A study of the solar chimney power plant systems, Journal of Engineering Thermodynamics 3, pp. 505-517, 2006.
15. C.B. Maia, A.G. Ferreira, R.M. Valle, M.F.B. Cortez, Theoretical evaluation of the influence of geometric parameters and materials on the behavior of the air flow in a solar chimney, Computers and Fluids 38, pp. 625-36, 2009.
16. T. Tahar, D. Mahfoud, Numerical Simulation of Natural Convection in a Solar Chimney, International Journal of renewable energy, pp. 713-716, 2012.
17. B.E. Launder, D.B. Spalding, The numerical computation of turbulent flow, Comput Meth Appl Mech Eng 3, pp. 269-289, 1974.
18. Fluent Inc. Fluent 6 manuals. Fluent Inc. ed. 2009.